Third International Symposium on Marine Propulsors
smp'13, Launceston, Tasmania, Australia, May 2013

Development of a shape-adaptive composite propeller using bend-twist coupling characteristics of composites

Manudha T. Herath[1*], B. Gangadhara Prusty[1], G. H. Yeoh[1], M. Chowdhury[1] and Nigel St. John[2]

[1] School of Mechanical and manufacturing Engineering, University of New South Wales, Sydney, Australia
[2] Maritime Platforms Division, Defence Science and Technology Organisation (DSTO), Fisherman's Bend, Victoria
*Corresponding Author. Email: m.herath@unsw.edu.au

ABSTRACT

An essential part in the development of composite marine propellers primarily focuses on the testing and understanding of their coupled fluid and structural behaviour. Due to economic and time limitations it is preferable to use computer simulation based results with satisfactory validation. Validation study for a twisted bend-twist coupled hydrofoil using experiments has been carried out using finite element (FE) based fluid structure interaction (FSI). Modelling and solution procedures using FSI are discussed to highlight the benefit of optimised designs using bend-twist coupling.

Keywords

Fluid-Structure Interaction, Composites, Marine Propeller, Bend-Twist coupling, Fiber Bragg Grating Strain Measurements

1 INTRODUCTION

Traditionally marine propellers are manufactured using Nickel Aluminium Bronze (NAB) alloys or Manganese Nickel Aluminium Bronze (MAB) alloys. However, more recently, usage of composites to manufacture marine propeller has been extensively investigated and attempted in practice. This is mainly due to favourable qualities of composites over metal alloys. Some of the significant advantages of composites over alloys can be listed as: light weight, reduced corrosion, reduced noise generation, no magnetic signature and shape adaptability (Mulcahy et al., 2011, Young, 2007, Mulcahy et al., 2010).

The advantage of shape adaptability is probably the most widely researched area in composite propellers over the past decade. Shape adaptability refers to the capability of composites to be optimised to deform, without the involvement of external mechanisms such as in controllable pitch propellers, based on the flow conditions and rotational speed in order to achieve a higher efficiency, compared to alloy propellers, throughout its operating domain. This is achieved through optimising the layup patterns and layup materials of the composite, such that the propeller has an optimum bend-twist coupling performance.

Bend-twist coupling refers to the special characteristic of layered composites where out of plane bending moments cause twisting moments in a composite structure. This special characteristic of composites has been attempted and exploited by various researchers in the past (Lee and Lin, 2004, Liu and Young, 2009, Motley and Young, 2011, Mulcahy et al., 2011, Young, 2007) to design a marine propeller that has the capability of self-varying pitch (shape adaptable) based on out of plane bending moments caused by the incoming flow.

However, designing a shape-adaptable composite propeller is significantly more complicated compared to designing a fixed pitch alloy marine propeller. Thus, the approach presented in this paper is to incrementally approach the problem by first attempting on bend-twist coupled hydrofoils. One of the main difficulties in the design process is conducting experiments that capture measurements in both fluid and structural domains. Furthermore, due to economic, time and resource constraints conducting water tunnel experiments may not be feasible for many researchers. Thus, the requirement for an accurate numerical model, which uses the fluid structure interaction (FSI) capabilities of modern finite element (FE) software, arises.

This paper is primarily focussed on using FSI capabilities of FEM using commercially available software ANSYS 14.0 to predict the response of a flexible composite hydrofoil blade. First, the paper briefly presents a validation study of FSI based on a published benchmarking procedure. Next, the theoretical background of bend-twist coupling is briefly explained taking the lift improvement of a simple NACA hydrofoil as an example. Finally, the experimental setup is explained drawing a comparison between measured experimental results for hydrofoil using fibre bragg gratings and predicted FSI results. The close agreement of the results demonstrates the capability of using FSI for a full scale composite propeller analysis.

2 FLUID-STRUCTURE INTERACTION

Fluid structure interaction is a rather complex branch in structural mechanics; thus, most fluid-structure interaction problems depend on numerical methods and

approximations. The basis of fluid-structure interaction is that the fluid domain is solved based on general fluid models and the structural domain is solved based on governing equations of the structure such that the normal stresses and velocities at the interface are balanced (Equations (1) and (2)) (Turek and Hron, 2006). Thus, the solution process is almost completely based on iterations over a large number of load steps and time steps. FSI simulations presented in this paper are bi-directional. Bi-directional is referred to the iterative process where both structural and fluid domains are solved through simultaneous iterations while maintaining the equilibrium conditions at the interface. Although this process requires a large computation time, it is more accurate compared to a uni-directional technique.

$$\boldsymbol{\sigma}^f . \hat{\boldsymbol{n}} = \boldsymbol{\sigma}^s . \hat{\boldsymbol{n}} \quad (1)$$

$$\boldsymbol{v}^f = \boldsymbol{v}^s \quad (2)$$

The model to validate the FSI technique is based on the FSI benchmarking model presented by Turek and Hron (2006). This is a simple model in which a flexible beam is placed in the wake of a cylindrical cavity. The asymmetric placement of the cylindrical cavity in the fluid domain (Figure 1) causes oscillatory flow patterns in the wake of the cylinder which in turn cause the flexible beam to oscillate and eventually settle at a steady state deflection.

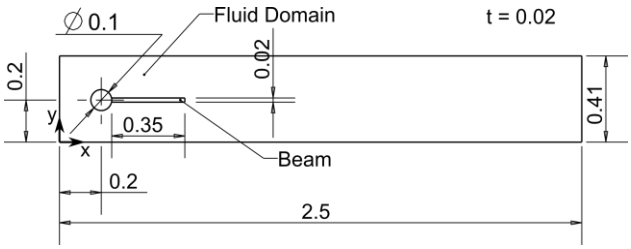

Figure 1: FSI validation model (all dimensions in meters)

A parabolic velocity distribution given by, $v_x(0, y) = \frac{0.3y(0.41-y)}{0.205^2}\, ms^{-1}$. This was applied at the inlet (left-hand edge); while, the outlet (right-hand edge) was considered to be in atmospheric pressure. All other boundaries were specified as a smooth wall boundary condition with no slip. Furthermore, the advection terms discretisation was set to "High Resolution" while Transient terms were discretised using Backward Euler Method. The "High Resolution" advection scheme in ANSYS CFX utilises an algorithm where required variable values at integration points are calculated based on more than one nodal values around the required integration point (ANSYS, 2011). The Second Order Backward Euler discretisation is robust, second order accurate in time and does not have time step selection limitations. The solution was set for 30s in the physical time domain with time step size of 0.02s. The maximum number of iterations per time step for the fluid domain was set to 100 for each time step and the residual root mean square target was set to 10^{-5}. In addition, fluid-solid interface load convergence target was set to 10^{-2} with a maximum number of interface load iterations of 50. Properties of the fluid medium and structure are given in Table 1. The flow was assumed to be laminar as the Reynolds Number of 20 around the cylinder is fairly low. The deformation of the structure is shown in Figure 2 and the results compared with the published results are presented in Table 2.

Table 1: Material properties used for the FSI simulation of validation model (Turek and Hron, 2006)

Property	Structure	Fluid
Density (kgm^{-3})	1000	1000
Poisson's Ratio	0.4	-
Shear Modulus (MPa)	0.5	-
Kinematic Viscosity (10^{-3} m^2s^{-1})	-	1

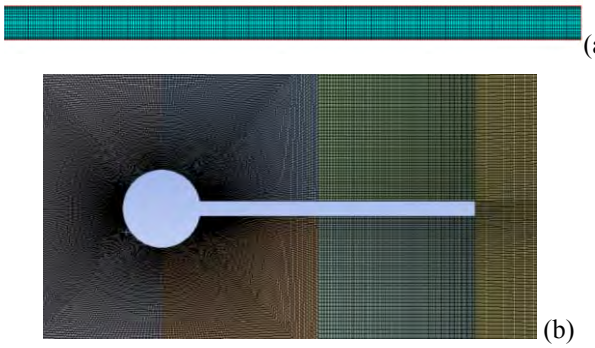

Figure 2: FE models: (a) Structural Domain, (b) Fluid Domain in the vicinity of the interface and (c) Generated flow velocity pattern and deformation of the structural beam

Table 2: Comparison of FSI results for validation model

	Reference (Turek and Hron, 2006)	ANSYS FSI	% Deviation
Deflection (mm)	0.82	0.89	6.8%
Lift (N/m)	0.76	0.74	3.4%
Drag (N/m)	14.29	14.27	0.2%

The marginal deviation between the results can be attributed to two main differences between the Turek and Hron (2006) 2-dimensional model and the FSI simulation. First, due to the used fluid domain solver (ANSYS CFX) that does not permit pure 2-dimensional solving, an infinitesimal thickness to the model was assigned, making both solid and fluid domains 3-dimensional. The second, is due to the iteration time-steps chosen to solve the model was 10 times larger than the times-steps used in the reference (Turek and Hron, 2006) ($\Delta t = 0.002\ s$ vs $\Delta t = 0.02\ s$). This modification was

introduced in the current analysis due to the limitations of computing capacity available. Considering these modifications, the correlation between the results can be considered satisfactory.

2.1 FSI results of a composite hydrofoil

The concept of using bend-twist coupled characteristics in a propeller blade is to promote optimum pitch change based on the bending moments caused by the incoming fluid flow. The determination of layup configuration to achieve such an optimum twist performance is dependent on a robust optimisation scheme (Herath and Prusty, 2012). One of the main requirements of the optimisation scheme is that the composite propeller reaches the shape of the optimum fixed-pitch (alloy) propeller at the operating condition (cruise condition). The use of FSI is primarily involved in this step where the unloaded shape of the composite propeller blade has to be calculated after the ply optimisation scheme has determined the ply configuration to enable the required twist variation. Unloaded shape calculation can be summarised in Figure 3.

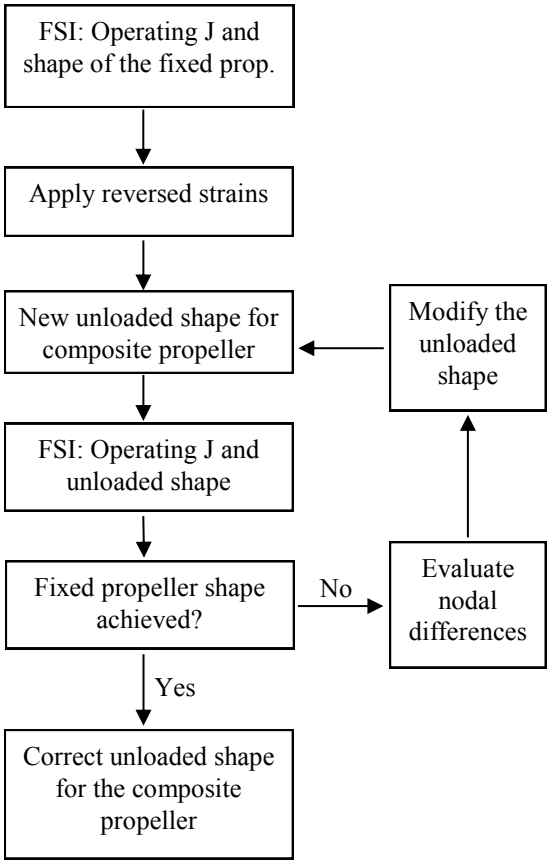

Figure 3: FSI concept for calculating the unloaded shape

However, the scope of this section is limited to demonstrating the use of bend-twist coupling of composites to achieve a required goal and demonstrating its effectiveness and feasibility of using FSI on composites.

The structure was modelled as a standard NACA 0012 aerofoil in a fluid (water at 25 ^{0}C) domain with an inlet speed of 4 ms^{-1} at an angle of attack (AoA) of 5^0. For these models a Shear Stress Transport (SST) turbulence model was picked as the flow was chosen to be significantly faster than that in the aforementioned verification model. Three models were created and lift generation was investigated – NAB, cross-ply composite (bend-twist uncoupled) and bend-twist coupled composite. All these modes were constructed with bi-directional coupling between fluid and structural domains to maintain similarity.

The composite laminate was taken as being constructed using LY556 epoxy reinforced with unidirectional E-glass 21xK43 Gevetex layers with a fibre volume fraction of 0.62. The principal material properties are given in Table 3 (Soden et al., 1998). Figure 4 illustrates the dimensions of the two domains.

Table 3: Mechanical Properties of the materials (Soden et al., 1998)

Property	21xK43/LY556	NAB
Density (kgm^{-3})	1850	7600
E_1 (GPa)	126	120
E_2 (GPa)	11	120
G_{12} (MPa)	6.6	42.3
ν_{12}	0.28	0.3
ν_{23}	0.4	0.3
Nominal Thickness (mm)	0.225	-

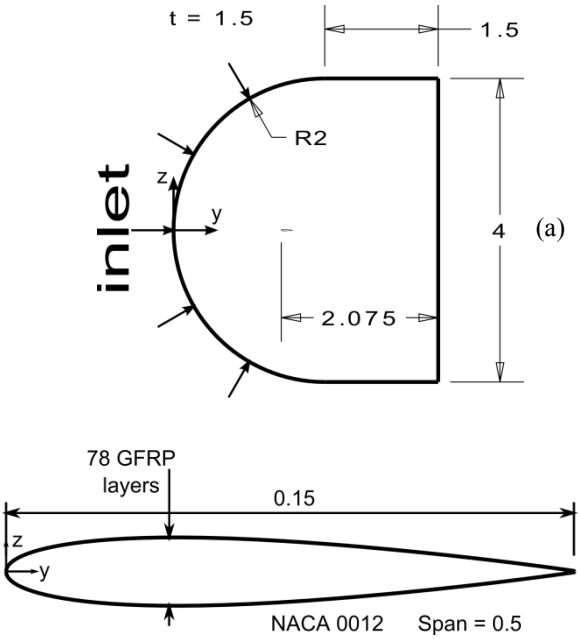

Figure 4: Dimensions (m) of the Model; (a) Fluid Domain, (b) Structural Domain

The two composite models were created with one having an uncoupled bend-twist characteristics and the other having coupled bend-twist characteristics. The uncoupled model was created with cross-ply laminates with a layup of $[(0/0/90)_{13}]_s$, while the coupled laminate was created with a layup of $[(30)_{78}]$. The resulting bending stiffness

([D]) and compliance ($[d] = [D]^{-1}$) matrices (assuming classical laminate theory) for these two layup configurations are,

$$[D_{UC}] = \begin{bmatrix} 19.61 & 2.275 & 0 \\ 2.275 & 13.26 & 0 \\ 0 & 0 & 2.626 \end{bmatrix} kN.m \ ;$$
$$[d_{UC}] = \begin{bmatrix} 52.04 & -8.925 & 0 \\ -8.925 & 76.92 & 0 \\ 0 & 0 & 330.8 \end{bmatrix} \mu \ N^{-1}m^{-1} \quad (3)$$

$$[D_c] = \begin{bmatrix} 17.22 & 5.615 & 5.502 \\ 5.615 & 8.968 & 1.645 \\ 5.502 & 1.645 & 2.898 \end{bmatrix} kN.m \ ;$$
$$[d_C] = \begin{bmatrix} 166.6 & -51.7 & -287 \\ -51.7 & 140.5 & 18.4 \\ -287 & 18.4 & 879.4 \end{bmatrix} \mu \ N^{-1}m^{-1} \quad (4)$$

Thus, for the bend-twist coupled layup, the twist is given by,

$$\kappa_{xy} = \left[-287M_x + 18.4M_y + 879.4M_{xy}\right] \times 10^{-6} \ m^{-1} \quad (5)$$

It must be noted that in this situation M_x is the dominant moment due to the lift in the z-direction. The layup configuration was in fact specifically chosen such that the angle of attack at the tip is increased due to coupling. This requires a negative coefficient for M_x in eq. (5) based on coordinate system in Figure 4. Thus, the layup was chosen such that the coefficient d_{31} is negative. If it is desired to reduce the angle of attack (to reduce drag, delay wing-tip stall, etc.), it is possible to choose a layup pattern such that d_{31} is positive.

With these layup patterns the structural domains of the two composite models were meshed with layered brick (solid186) elements. Layered solid elements were chosen over layered shell elements as they can accurately model varying thicknesses of hydrofoils; especially, in the case of complex hydrofoils that will be investigated later in the research. Even in this model, although it has a relatively simple cross-section, use of layered solid elements can potentially improve the coupling accuracy between solid and fluid in comparison to using a shell layer with no real thickness. Furthermore, orientations and material properties of each composite layer was input to the system individually rather than using one layer with an equivalent orientation and an equivalent set of material properties. Therefore, this model has the potential to provide more accurate results compared to the models presented in (Marine, 1993, Lin and Lee, 2004, Mulcahy et al., 2011, Young, 2008, Young, 2007). However, the main drawback of using brick elements is that the nodes of brick elements do not have rotational degrees of freedom; thus, it is required to generate a fine mesh in order to accurately capture nodal rotations.

Figure 5 and Figure 6 illustrate the final results that were obtained. Comparison of the lift forces obtained for the three different models is presented in Table 4.

Table 4: Comparison between lift and drag results for NACA 0012 hydrofoil

Entity	NAB	Cross-Ply	B-T coupled
Lift (N)	215.83	217.39	223.56
% Lift increase	0%	0.72%	3.58%

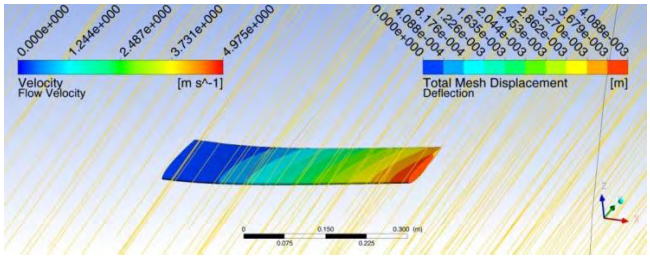

Figure 5: Flow pattern and the twist of the bend-twist coupled hydrofoil

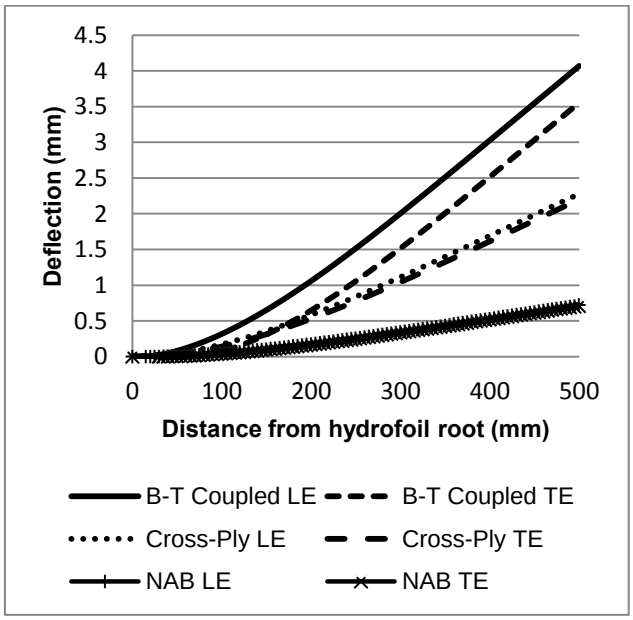

Figure 6: Deflections at the leading edge and trailing edge

Based on the above results it is clear that it is possible to gain a clear advantage in terms of lift force by using properly bend-twist coupled laminates. In addition, the two composite models are 75.7% lighter compared to the NAB model. Although the increase of lift in this model is just 3.58%, by proper optimization it may be possible to gain an even higher lift. Furthermore, it is possible to optimize bend-twist coupling in order to cater many requirements such as reducing drag, delaying wing-tip stall, increasing stability, increasing lift/drag ratio, etc (Reddy, 2004).

3 MODEL GENERATION

Specifics of the experimental model and the finite element model will be discussed. The creation of the experimental model and the finite element model will be discussed in detail followed by an explanation about the experimental conditions and parameters of the finite element model.

3.1 Experimental Specimen

The response of a composite hydrofoil under fluid loading was experimentally measured by DSTO at the cavitation tunnel facility of Australian Maritime College, Tasmania (Davis et al., 2012). The hydrofoil chosen for the experiments was a result of the optimization process carried out by Mulcahy et al. (2011).

The optimization process was formulated such that the hydrofoil straightens, whereby reaching its optimum shape at the operating condition. Thus, a pre-deformation was introduced at the unloaded condition. Due to the pre-deformation, tip of the hydrofoil was dropped 8.3 mm and twisted 1.2° relative to the root (Mulcahy et al., 2009). The profile of the hydrofoil conformed to the NACA 00xx series with a non-linear maximum thickness variation at each cross-section (at 0.3 × chord) as given in Table 5. The thickness variation was evaluated by a trial-and-error method based on maintaining both the required flexibility and strength simultaneously (Mulcahy et al., 2009). Ply termination was introduced at the innermost plies to account for the thickness variation along the span.

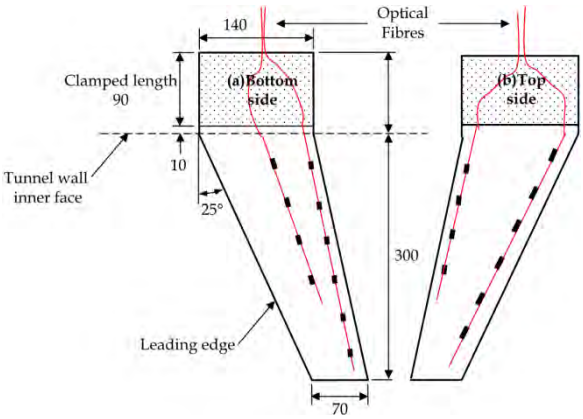

Figure 7: Hydrofoil dimensions and setup (Davis et al., 2012)

Table 5: Thickness variation of the hydrofoil (Mulcahy et al., 2009)

Distance from wall (mm)	Max. thickness (mm)
0	15.0
30	14.6
60	13.7
90	12.2
120	10.3
150	8.4
180	7.0
210	6.0
240	5.4
270	5.1
300	5.0

Strain measurements were taken using Fibre Bragg Grating (FBG) sensors embedded to the outermost GFRP layer of the hydrofoil (Davis et al., 2012). The composite specimen was manufactured using Resin Transfer Moulding (RTM) by DSTO as shown in Figure 8.

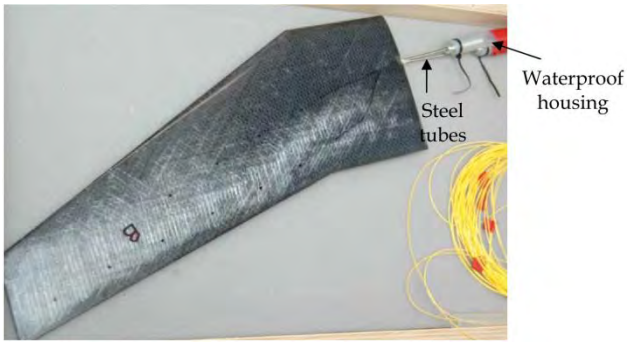

Figure 8: Manufactured Hydrofoil (Davis et al., 2012)

The foil was manufactured using a hybrid layup of 0/90 glass fibre fabric and unidirectional carbon fibre layers and an epoxy resin matrix. The layup pattern at the maximum thickness of the foil (root) was $[0^G/45^G/70^C/((70^C)_2/0^G/(70^C)_2/45^G)_2/(70^C)_2/0^G/70^C]_s$.

Material properties (Table 6) were based on coupon testing conducted as a part of the experimental program (Mulcahy et al., 2009).

Table 6: Properties of composite layers (Mulcahy et al., 2009)

	Glass Fabric / Epoxy	Carbon Fibre / Epoxy
E_{11} (GPa)	20.6	117.9
E_{22} (GPa)	20.6	6.55
ν_{12}	0.32	0.27
G_{12} (GPa)	4.14	4.82
G_{23} (GPa)	4.14	3.75
G_{13} (GPa)	4.14	4.82

3.2 Finite Element Model

Finite element simulations were performed using the commercial FEA software, ANSYS 14.0 as bi-directional FSI with both structural and fluid solvers running at transient state. It was attempted to create the FE model as accurately as possible compared to the experimental model and replicate experimental conditions.

The structural domain was created using 20-node layered brick elements (solid186) spanning out from the centre (core) of the hydrofoil towards the surface. Brick elements were used as opposed to shell elements due to the varying thickness and complex geometry of the hydrofoil. Ply termination was modelled using span-wise partitioning of the model and specifying the ply layup based on the mean thickness of each partition. Figure 9 demonstrates the layup pattern of both experimental and FE models at the tip.

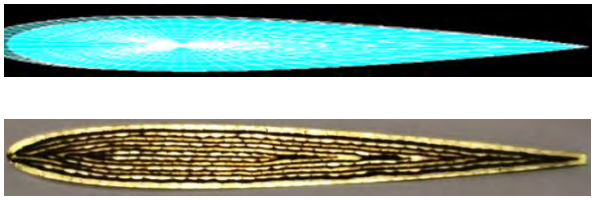

(a)

(b)

Figure 9: Layup pattern of the hydrofoils; (a) Finite Element model, (b) Experimental Specimen

The fluid domain was constructed to be identical to the water tunnel test area with a 0.6 m x 0.6 m x 2.6 m. Similar to the verification model, the advection terms were discretised using the "High Resolution" algorithm in CFX while the transient terms were discretised using Second Order Backward Euler discretisation (with $\Delta t = 0.1\ s$). Furthermore, turbulence numerics were discretised using First Order scheme due to easier convergence and faster solution.

Experiments were conducted at three different flow conditions – Re = 0.5×10^6, 1×10^6 and 1.5×10^6 (water at 20 °C taking root chord as the reference length) with AoAs at root varying from -15° to 15° (Davis et al., 2012). For the purposes of this paper and due to computing limitations, simulations were performed only at Re = 0.5×10^6 at an angle of attack of 5°. Three fluid models were used for comparison purposes: laminar, Shear Stress Transport (SST) turbulence model, BSL Reynolds Stress (BSL RS) turbulence model and k-Epsilon turbulence models. Two fluid domain meshes (predominantly using 8-noded fluid elements) were created with one having with approximately 3.5 million nodes (approximately 4 million cells) and the other having approximately 1 million nodes (approximately 1.2 million cells). Figure 10 shows the mesh around the hydrofoil of the finer mesh. Although there were differences in strain results obtained using these two models, they were not significant. Results discussed in the following sections were obtained using the finer mesh model.

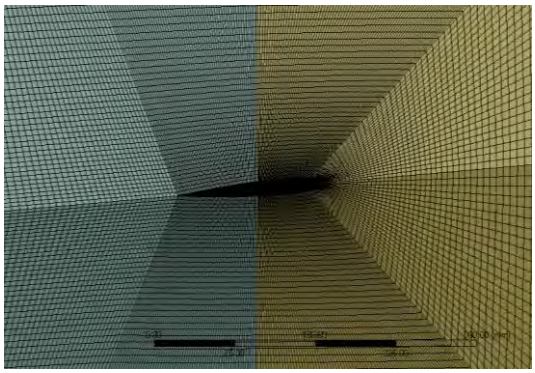

Figure 10: Fluid domain cross-section in the vicinity of the hydrofoil

4 RESULTS AND DISCUSSION

During experiments strain results along three FBG arrays were documented. Thus, finite element results will be presented for three FBG arrays and will be compared against experimental results. Measurements from three FBG arrays were taken during experiments (Figure 11):

1. 20 mm from the trailing edge, bottom side of the foil (6 FBGs)
2. 20 mm from the trailing edge, top side of the foil (4 FBGs)
3. 20 mm from the leading edge, top side of the foil (6 FBGs)

Measurements from the fourth array (array at the bottom centre in Figure 7) were not recorded due to a technical fault during setup. The FBGs were spaced approximately 50 mm apart and were stitched to the outermost fibre glass layer. Accordingly, in the FE model the results were obtained by appropriately orienting local coordinate systems in the direction of the fibres and calculating directional strains.

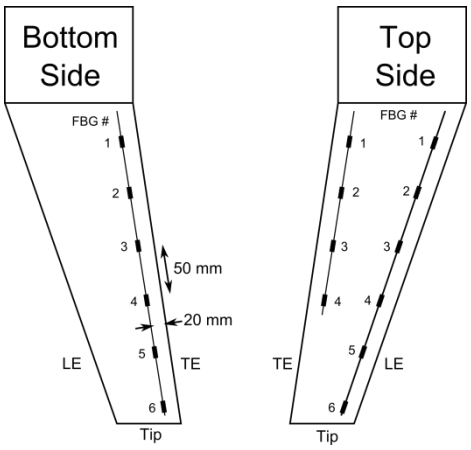

Figure 11: FBG array setup

4.1 Strain Results

It was observed that the use of turbulence models did not make a significant change to the strain results. However, BSL Reynolds Stress turbulence was witnessed to produce slightly better results compared to laminar flow model, SST model and k-Epsilon model. Figure 11 shows the comparison between experimental results and FSI strain results obtained using the BSL RS model.

Comparison between results can be considered satisfactory. Although the difference was minute, there was a slight improvement in using BSL RS turbulence model. SST and k-Epsilon models produced results almost identical to the Laminar Model in terms of structural deflections. It may be possible to observe larger differences at higher flow speeds.

It was witnessed that the numerical model repeatedly overestimated strains close to the clamped edge of the hydrofoil. At this stage, it is assumed that this is due to numerical singularities in the vicinity of the clamped edge and due to the imperfect nature of a practical clamp compared to an ideal fixed support in FEA. However, this will be investigated in the future with the intention of further improving the model. In addition, it is documented by Davis et al. (2012) that vibrations of approximately 33Hz were observed during experiments. However, this was not captured by the FSI simulations. Accordingly, future investigations will be focused towards the damping of the hydrofoil and simulations will be performed at a relatively smaller time-step to accurately capture vibrations.

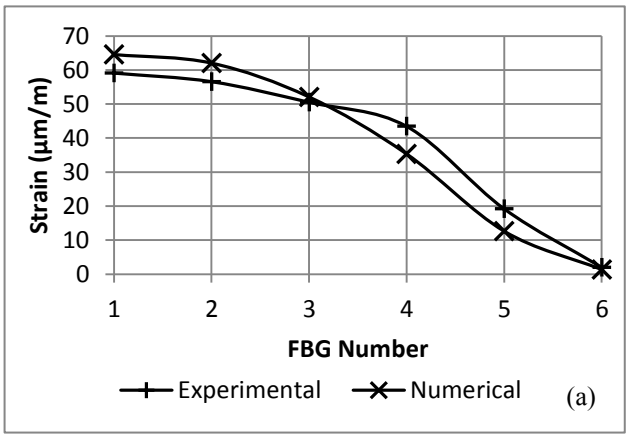

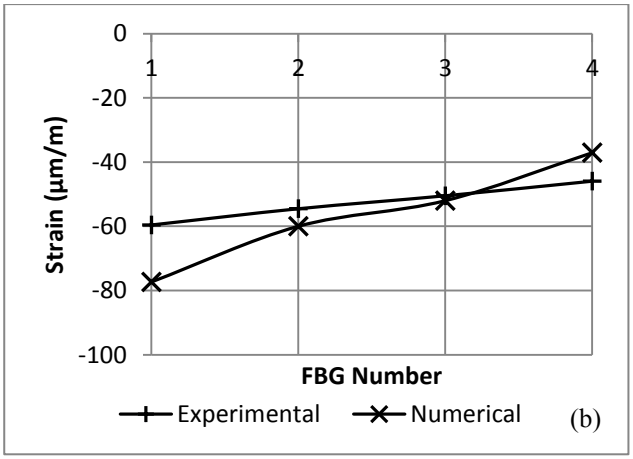

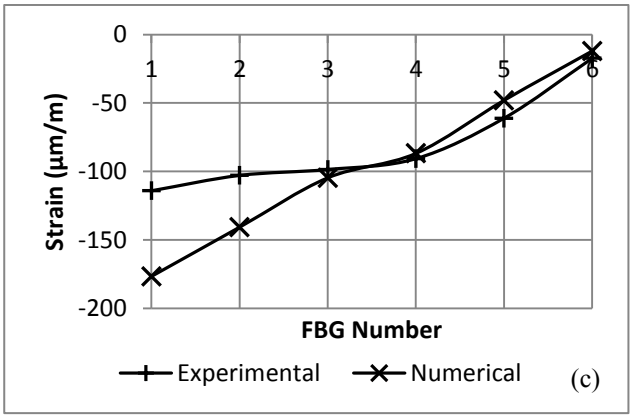

Figure 12: Results comparisons for FBG arrays; (a) Trailing Edge Bottom, (b) Trailing Edge Top, (c) Leading Edge Top

4.2 Hydrodynamic Results

As a part of the experiments hydrodynamic results were not documented. However, with the confidence gained through the above verification, following results were evaluated using FEA. Following table draws a comparison between pure CFD (equivalent to a rigid hydrofoil) measurements and FSI measurements.

Table 7: Lift and Drag results

	CFD	FSI
Lift (N)	63.17	62.78
Drag (N)	4.76	4.69
L/D	13.28	13.39

The slight increase in L/D is a result of the optimisation performed by Mulcahy et al. (2011). As stated earlier, the layup was chosen such that the L/D ratio is reduced compared to the rigid hydrofoil. Thus, the FSI results conform to the predictions and objectives of the optimisation scheme. However, the notably small difference between L/D by CFD and FSI is due to the fact that experiments were not conducted at the optimum design flow speed of the hydrofoil. In other words, the hydrofoil was not operating at its optimum performance.

5 CONCLUSION

The work presented in this paper sets fundamental but essential knowledge to investigate shape-adaptable composite marine propellers. The paper presented a validation study that compares results obtained numerically using Fluid-Structure Interaction of Finite Element Analysis and experimental results. Although several simplifications were made for modelling purposes the consistency between FEA and experimental results are in good agreement. The knowledge gained through this validation study is extremely helpful in developing an optimisation scheme and an accompanying numerical model that can accurately predict the performance of optimised designs without the need for extensive experimentations.

6 ACKNOWLEDGEMENTS

Authors would like to sincerely thank DSTO for the composite foil results, especially acknowledging Dr Claire Davis and her team on the Bragg strain sensor work, Russell Cairns for the foil manufacture and David Clark for the conduct of cavitation tunnel tests.. Also thanks to Dr Lex Mulcahy from Pacific ESI for his continued support and guidance.

7 REFERENCES

Ansys (2011). 'CFX-Solver Theory Guide Canonsburg', PA, USA: ANSYS Inc.

Davis, C., Norman, P., Kopczyk, J. & Rowlands, D. (2012). 'Initial Trial using Embedded Fibre Bragg Gratings for Distributed Strain Monitoring in a Shape Adaptive Composite Foil' Fishermans Bend, Victoria: Defence Science and Technology Organisation.

Lee, Y.-J. & Lin, C.-C. (2004). 'Optimized Design of Composite Propeller'. Mechanics of Advanced Materials and Structures, 11, 17-30.

Lin, C.-C. & Lee, Y.-J. (2004). 'Stacking sequence optimization of laminated composite structures using genetic algorithm with local improvement'. Composite Structures, 63, 339-345.

Liu, Z. & Young, Y. L. (2009). 'Utilization of bend–twist coupling for performance enhancement of composite marine propellers'. Journal of Fluids and Structures, 25, 1102-1116.

Marine (1993). 'Composites offer advantages for propellers'. Reinforced Plastics, 37, 24-26.

Motley, M. R. & Young, Y. L. (2011). 'Performance-based design and analysis of flexible composite propulsors'. Journal of Fluids and Structures, 27, 1310-1325.

Mulcahy, L., Anderson, B., Widjaja, R. & Gardiner, C. P. (2009). 'Composite Shape-Adaptive Technology for Marine Propellers'. Cooperative Research Centre for Advanced Composite Structures Limited.

Mulcahy, N. L., Prusty, B. G. & Gardiner, C. (2010). 'Hydroelastic design of composite components'. International Journal of Ship and Offshore Structures, 5, 359-370.

Mulcahy, N. L., Prusty, B. G. & Gardiner, C. P. (2011). 'Flexible composite hydrofoils and propeller blades'. Transactions of the Royal Institution of Naval Architects Part B: International Journal of Small Craft Technology, 153, B39-B46.

Reddy, J. N. (2004). Mechanics of Laminated Composite Plates and Shells: Theory and Analysis, Boca Raton, Florida, USA, CRC Press.

Soden, P. D., Hinton, M. J. & Kaddour, A. S. (1998). 'Lamina properties, lay-up configurations and loading conditions for a range of fibre-reinforced composite laminates'. Composites Science and Technology, 58, 1011-1022.

Turek, S. & Hron, J. (2006). 'Proposal for numerical benchmarking of fluid-structure interaction between an elastic object and laminar incompressible flow'. *In:* Bungartz, H. & Schäfer, M. (eds.) Lecture Notes in Computational Science and Engineering. 1st Ed. ed.: Springer.

Young, Y. L. (2007). 'Hydroelastic Behavior of Flexible Composite Propellers in Wake Inflow'. 16th International Conference on Composite Materials Kyoto, Japan.

Young, Y. L. (2008). 'Fluid–structure interaction analysis of flexible composite marine propellers'. Journal of Fluids and Structures, 24, 799-818.